Translocator proteins: Scarf and Kassiou provide an overview on TSPOs and the use of PET radioligands to track progression and severity of neuroinflammatory disease and other pathologies. . . . . ***Page 677***

Patient release and ^{131}I therapy: Goldsmith questions current regulatory restrictions focused on release of patients after radioiodine therapy and previews an article in this issue of *JNM* on health care challenges posed by these requirements. . . . . .***Page 681***

Delayed ^{131}I therapy and survival: Higashi and colleagues explore the clinical factors affecting survival of patients with differentiated thyroid carcinoma after total thyroidectomy. . . . . ***Page 683***

^{18}F-FLT PET and lymphoma prognosis: Herrmann and colleagues correlate initial uptake of ^{18}F-FLT with clinical outcomes in patients with aggressive non-Hodgkin lymphoma treated with rituximab, cyclophosphamide, doxorubicine, vincristine, and prednisone. . . . . ***Page 690***

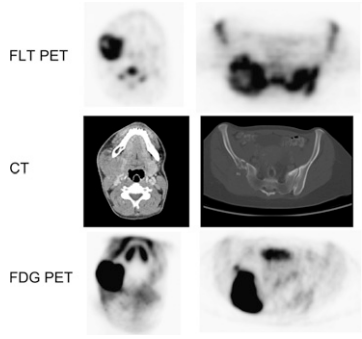

Single CT phases in PET/CT: Ruf and colleagues assess the value of each CT phase (early arterial, portal–venous inflow, and venous) of a triple-phase CT protocol in comparison with ^{68}Ga-DOTATOC PET in diagnosing neuroendocrine tumors. . . . . .***Page 697***

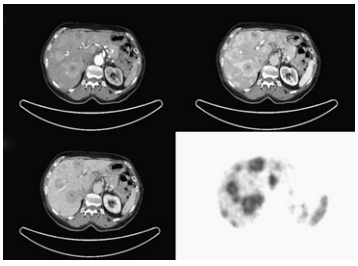

^{18}F-FDG PET biology in metastatic tumors: Kaira and colleagues investigate the underlying biologic mechanisms of ^{18}F-FDG uptake in metastatic pulmonary tumors to more fully understand the ability of PET to predict therapeutic response and outcomes. . . . . ***Page 705***

Lesion detection in TOF PET: Surti and colleagues evaluate the benefit of fully 3D time-of-flight PET in clinical whole-body oncology using human observers to localize and detect lesions in realistic patient anatomic backgrounds. . . . . ***Page 712***

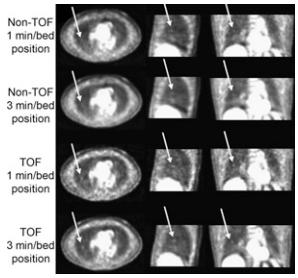

Clinical apoptosis imaging: Höglund and colleagues detail the first-in-humans study with ^{8}F-ML-10, a small-molecule PET tracer for apoptosis. . . . . ***Page 720***

Myocardial flow reserve and prognosis: Fukushima and colleagues describe prediction of short-term cardiovascular events using quantification of global myocardial flow reserve in patients referred for clinical ^{82}Rb PET perfusion imaging. . . ***Page 726***

Combined tracers in degenerative Parkinsonism: Südmeyer and colleagues report on the combined ability of ^{123}I-labeled IBZM, FP-CIT, and MIBG SPECT and a multidimensional statistical algorithm to distinguish idiopathic Parkinson disease from atypical parkinsonian disorder. . . . . ***Page 733***

Prostate sentinel nodes: Vermeeren and colleagues evaluate a portable γ-camera for sentinel node identification during laparoscopic sentinel lymphadenectomy for prostate cancer. . . . . ***Page 741***

Parametric viability images with ^{15}O-H_2O: Harms and colleagues describe the generation of parametric perfusable tissue index images from a ^{15}O-H_2O PET/CT scan without an additional ^{15}O-CO scan. . . . . ***Page 745***

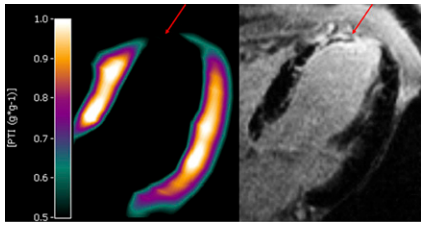

MPI and preoperative risk stratification: Weinstein and Steingart provide an educational overview of the role of myocardial perfusion imaging in preoperative risk assessment and make recommendations for integration of current guidelines into clinical practice. . . . . ***Page 750***

Model of old myocardial infarction: Teramoto and colleagues describe PET studies assessing the pathophysiologic status of a pig model of reduced left ventricular function and remodeling with long survival after myocardial infarction. . . . ***Page 761***

Small-animal PET/CT in osteoporosis: Li and colleagues use PET/CT to analyze the impact of estrogen deficiency osteoporosis on microdamage by observing changes in the uptake of ^{18}F-fluoride in

the tibiae of ovariectomized rats after fatigue loading. . . . . ***Page 769***

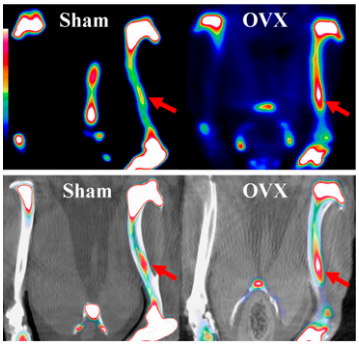

Enhancing ^{111}In-DTPA-hEGF therapy: Cornelissen and colleagues investigate whether the therapeutic efficacy of ^{111}In-labeled human epidermal growth factor is increased by coadministration of selected molecularly targeted drugs that modulate EGF receptor signaling and trafficking. . . . . ***Page 776***

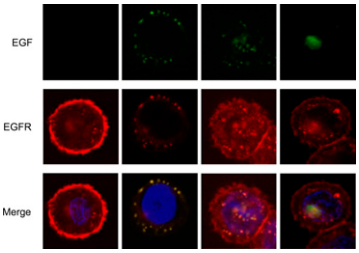

Imaging intraprostatic gene transcription: Pouliot and colleagues combine a novel transcriptional amplification system signal with a protocol for tracer administration to demonstrate in vivo PET detection of transcriptional activity in both mouse and immunocompetent canine prostates. . . . . ***Page 784***

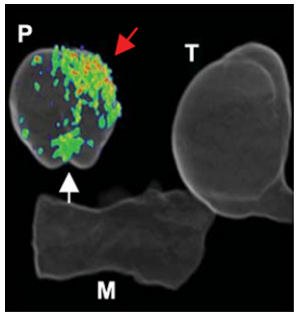

Small-animal PET of tumor damage: Song and colleagues investigate the potential application of small-molecular-weight ^{64}Cu-labeled bis-DOTA-hypericin for noninvasive assessment of response to photothermal ablation therapy. . . . . ***Page 792***

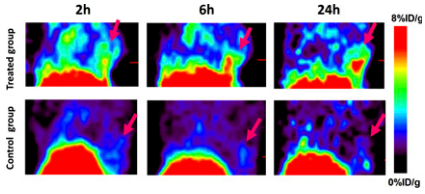

Kinetics and uptake of ^{18}F-FDG in mice: Wong and colleagues explore the effects of dietary condition, blood glucose level, and injection site on kinetics and uptake of ^{18}F-FDG in mice. . . . . ***Page 800***

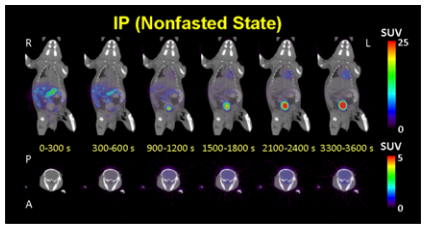

^{18}F-FBnTP and BAT thermogenesis: Madar and colleagues report on an approach to detect brown adipose tissue depots and monitor thermogenesis using a mitochondria-targeting, voltage-sensing PET tracer. . . . . ***Page 808***

β-Camera with a microfluidic chip: Vu and colleagues describe an integrated β-camera and microfluidic chip capable of quantitative imaging of glycolysis radioassays using ^{18}F-FDG in small cell populations down to a single cell. . . ***Page 815***

Transport and fate of anti–^{18}F-FACBC: Okudaira and colleagues provide experimental data clarifying the transport mechanism of this amino acid PET tracer in prostate cancer cells and describe its promise for clinical imaging. . . . . ***Page 822***

Opinions about RIT: Schaefer and colleagues report on the results of a survey of nuclear medicine and radiation oncology professionals on opinions and patterns of use of ^{90}Y-ibritumomab tiuxetan and ^{131}I-tositumomab radioimmunotherapy. . . . . ***Page 830***

ON THE COVER

Laparoscopic use of a portable γ-camera to identify sentinel nodes during sentinel lymphadenectomy for prostate cancer leads to excision of more radioactive nodes and can determine the residual radioactivity after excision. The image at bottom confirms adequate excision of the sentinel nodes that were identified in the image at top. The injection area is seen caudally in both images.

See pages 742 and 743.